Water and polymer dynamics in a model polysaccharide hydrogel: the role of hydrophobic/hydrophilic balance

B. Rossi,*[ab] V. Venuti,[c] F. D'Amico,[a] A. Gessini,[a] F. Castiglione,[d] A. Mele,[de] C. Punta,[d] L. Melone,[d] V. Crupi,[c] D. Majolino,[c] F. Trotta[f] and C. Masciovecchio[a]

Received 9th September 2014,
Accepted 10th November 2014

Introduction

Polymer-based gels are ubiquitous in nature and in many commonly used materials. Polymeric hydrogels can be formed by water swelling of three-dimensional networks involving either chemical or physical interactions.[1] In both cases, the grade of entanglement of the polymer structure, depending on its formulation and the proportions of ingredients, is mainly responsible for the swelling behaviour of the system.

In recent years, hydrogels have received significant attention due to their possible applications in the biomedical[2] and tissue engineering fields,[3,4] as scaffolds for cell growth,[5] and in drug delivery, as controlled outflow materials.[6–8]

[a] *Elettra - Sincrotrone Trieste, Strada Statale 14 km 163.5, Area Science Park, 34149 Trieste, Italy. E-mail: rossi@science.unitn.it*
[b] *Department of Physics, University of Trento, Via Sommarive 14, 38123 Povo, Trento, Italy*
[c] *Department of Physics and Earth Sciences, University of Messina, Viale Ferdinando Stagno D'Alcontres 31, 98166 Messina, Italy*
[d] *Department of Chemistry, Materials and Chemical Engineering "G. Natta", Politecnico di Milano, Piazza L. da Vinci 32, 20133 Milano, Italy*
[e] *CNR Istituto di Chimica del Riconoscimento Molecolare, Via L. Mancinelli, 7, 20131 Milano, Italy*
[f] *Department of Chemistry, University of Torino, Via Pietro Giuria 7, 10125 Torino, Italy*

The study of hydrogels offers a complex phenomenology for the coexistence of solid-like and liquid-like behaviour.[9,10] This is mainly due to the unique properties of the water solvent and due to the dynamics processes occurring in the system that entails motions of specific chemical groups of the polymer, water diffusion and matrix–solvent interactions. Giving an exhaustive description of these processes is a challenging task, especially because they occur over a very broad time and space scales. The detailed explanation of the structure and dynamics of hydrogel systems thus requires the combination of different and complementary physical methods suitable for the exploration of such different time and distance domains. For example, Scanning Electron Microscopy (SEM) has been widely used to capture images of the characteristic network structure in hydrogels,[11,12] while Infrared spectroscopy and Light Scattering techniques have been implemented for investigating the structural arrangement in hydrogels[13] and to determine the molecular distribution and parameters of the polymer matrix.[14,15] Additionally, rheology, NMR relaxometry measurements and neutron scattering experiments have been described in the literature as emerging methodologies used for the elucidation of the structural and viscoelastic properties of hydrogels.[16–19]

All these studies indicated that the balance between the hydrophilic/hydrophobic chemical groups and the degree of cross-linking of the polymer structure are key parameters which

allow us to control the equilibrium swelling in hydrogels and their water-retaining ability,[20] thus providing the physico-chemical bases for the design of efficient, smart hydrogel-based carriers and controlled release systems.[2]

With this picture in mind, an extensive, multidisciplinary investigation has been carried out in the recent years on a paradigmatic model of chemically cross-linked polymers, namely cyclodextrin nanosponges (CDNS), with the main goal of understanding the state and the molecular environment of water molecules within the 3D polymeric network in the hydrogel state.

CDNS are cross-linked polymers synthesized by condensation reaction of the OH groups of the glucose units of cyclodextrins (CD) with a poly-functional cross-linker agent (CL).[21,22] An example of the CL reagent used is pyromellitic anhydride (PMA). Some types of CDNS exhibit a marked and selective swelling behaviour when contacted with water or water solution only, affording hydrogels.[23–25]

Nanosponges have been shown to be promising nanoporous materials with interesting properties of sorption of both organic and inorganic molecular species. Several studies are present in the literature reporting on the performances of CDNS as efficient carriers for uses in agriculture,[26] environmental control[27] and for pharmaceutical applications.[21,22,28]

Besides their potential practical applications, nanosponges are interesting model systems for the study of water-swollen cross-linked polymers. Indeed, CDNS are characterized by a nanoporous structure with both hydrophilic and hydrophobic domains, corresponding to the carbohydrate nature of CDs and to the presence of the apolar cavity of the CD units, respectively. Additionally, the cross-linking reaction gives rise to hydrophilic pores of the growing polymer. All the recent experimental and theoretical studies consistently suggested that the cross-linking degree and the hydrophilicity/hydrophobicity of the final CDNS can be tuned by varying the chemical structure of the CL and the relative amount of CL with respect to the monomer CD (*i.e.* n = cross-linking agent in molar excess with respect to CD) during the synthesis.[29–33] In addition, the controlled ability to undergo modifications from the state of a rigid gel to liquid suspension has been recently evidenced in CDNS-based hydrogels by changing the hydration level of polymers in water.[25,34,35]

The main purpose of this work is to highlight the role played by the hydrophobic and hydrophilic groups of water-swollen CDNS in determining the gelation phenomena. To this aim, we combine the use of Raman and Infrared spectroscopy, exploiting the different and complementary sensitivity of these techniques to the vibration modes associated with the engaged water molecules and with the chemical groups of the polymer matrix. In particular, the use of UV Raman scattering gives the advantage to selectively study the vibrational modes associated with aromatic rings present in the CDNS structure obtained by using PMA as a cross-linker, whose Raman signal is enhanced in the spectra excited under UV light with respect to the visible radiation.[36]

The case study of the PMA-nanosponge hydrogel is presented here as a contribution to the comprehensive view of the molecular behaviour of the two main components of the hydrogel – water and the polymer – concurring to the resulting macroscopic properties of the gel. The modifications observed in the vibrational spectra of CDNS hydrogels will be monitored as a function of the hydration level of polymers and the molar ratio n used in the synthesis of nanosponges.

The overall results contribute to the atomic length scale description of the swelling phenomena, leading to the formation of the gel phase when a chemically cross-linked polymer contacts with water or biological fluids.

Experimental

A. Synthesis of cyclodextrin nanosponges

The nanosponges β-CDNSPMA1n were obtained following the synthetic procedure reported previously.[21] Anhydrous β-cyclodextrin (β-CD) was dissolved at room temperature in anhydrous DMSO containing anhydrous Et_3N. Then, the cross-linking agent pyromellitic anhydride (PMA) was added at 1 : n molar ratios (with n = 4, 6, 8, 10) under intense magnetic stirring. The polymerization was complete in few minutes resulting in a solid which was broken up with a spatula and washed with acetone in a Soxhlet apparatus for 24 h. The pale yellow solid was finally dried under vacuum. The corresponding hydrogels of CDNS were prepared by adding a suitable amount of double-distilled water (Sigma) to the dry samples in order to obtain the desired levels of hydration h. The hydration level h is defined as the weight ratio of H_2O/CDNS. All the gel samples were freshly prepared and used for Raman scattering and FTIR-ATR absorption measurements.

B. UV Raman scattering measurements and data analysis

UV Raman scattering measurements were carried out at the BL10.2-IUVS beamline at the Elettra Synchrotron laboratory in Trieste. A complete description of the experimental set-up can be found elsewhere.[36] The Raman spectra were excited at 266 nm and collected, at room temperature, in a back-scattered geometry using a triple stage spectrometer (Trivista, Princeton Instruments). The experimental resolution was set to 5 cm^{-1} in order to ensure enough resolving power and count-rate. To minimize the potential photodecomposition of the gels resulting from UV exposure, the sample cell was subjected to slow continuous spinning during the measurements in order to vary the position of the sample volume scattering through the beam. For each examined sample, four subsequent Raman spectra were recorded in order to verify their reproducibility and exclude any appreciable damage due to possible heating or photodecomposition of the gels.

By using polarizers and wave plates, we have collected the light inelastically diffused from the sample polarized parallel ($I_{\parallel}$) and perpendicular ($I_{\perp}$) with respect to the incident radiation. The isotropic Raman intensity has been obtained according to the relation $I_{iso} = I_{\parallel} - 4/3\ I_{\perp}$.

The fitting procedure of the isotropic Raman spectra have been carried out through a least squares minimization procedure, following the steps described in ref. 37 to ensure the

likelihood of the results. The isotropic Raman spectral lineshape can be represented by

$$I_{\mathrm{iso}} = \sum_{i=1}^{N} A_i K_i\left(\omega, \omega_0^i, \langle\omega^2\rangle^i, \tau_c^i\right) + B \qquad (1)$$

where A_i are the scaling factors and $K_i(\omega,\omega_0^i,\langle\omega^2\rangle^i,\tau_c^i)$ is the Kubo–Anderson Function (KAF). The latter function can be expressed by the following equation:

$$K_i\left(\omega, \omega_0^i, \langle\omega^2\rangle^i, \tau_c^i\right) \propto \frac{e^{\alpha_i{}^2}}{\alpha_i} \sum_{n=0}^{\infty} \frac{(-\alpha_i{}^2)}{n!} \frac{\alpha_i + n/\alpha_i}{(\alpha_i + n/\alpha_i)^2 + \frac{(\omega - \omega_0^i)^2}{\langle\omega_i{}^2\rangle}} \qquad (2)$$

where $\langle\omega_i{}^2\rangle$ is the variance of the frequency spread around the unperturbed frequency ω_0^i while $\alpha = (\langle\omega^2\rangle)^{1/2}\,\tau_c$.

Parameters α and τ_c represent, respectively, the spread in the central frequency and the characteristic decay time of a generic stochastic perturbation acting on the vibrating atoms. If these atoms are involved in hydrogen bonds, then α and τ_c are, respectively, the spread in the central frequency due to the schastic variance in the hydrogen bond geometry and lifetime.[37] In the limit $\alpha \ll 1$ (fast modulation limit) eqn (2) can be approximated by a Lorentzian function and parameter τ_c is related to the dephasing time τ_{deph} through the relation:

$$\tau_{\mathrm{deph}} = \frac{1}{\langle\omega^2\rangle\tau_c} \cong \frac{1}{\pi\Gamma} \qquad (3)$$

where Γ is the Lorentzian linewidth.

C. FTIR-ATR measurements

FTIR-ATR measurements were performed at T = 290 K on the hydrogel prepared by hydration of the corresponding dry samples of CDNS in water. The spectra were collected in the 400–4000 cm^{-1} wavenumber range on a Bomem DA8 Fourier transform spectrometer, operating with a Globar source, in combination with a KBr beamsplitter, a DTGS/KBr detector. The samples were contained in the Golden Gate diamond ATR system, just based on the ATR technique. The spectra were recorded in a dry atmosphere, in order to avoid dirty contributions, with a resolution of 4 cm^{-1}, automatically adding 100 repetitive scans in order to obtain a good signal-to-noise ratio and high reproducibility. All the IR spectra were normalized for taking into account the effective number of absorbers. No mathematical correction (*e.g.*, smoothing) was done, and spectroscopic manipulation such as baseline adjustment and normalization were performed using the Spectracalc software package GRAMS (Galactic Industries, Salem, NH, USA).

D. Quantum chemical computation

The molecular model of 1,2,4,5-tetracarboxybenzoic acid dimethyl ester[31] was built from scratch by using the PCMODEL 8.0 package (Serena Software, Bloomington, IN, USA) and allowed to fully relax in the MMX force field. The energy minimized geometry was in turn used as a starting structure for *ab initio* quantum chemical computations carried out using the GAUSSIAN 03 program suite and unrestricted Density Functional Theory (DFT).[38] Additional details can be found in ref. 31.

Results and discussion

Fig. 1(a) and (b) show the comparison between the experimental Raman and IR profiles acquired for the β-CDPMA14 nanosponge polymer and the theoretical Raman activity and infrared intensities obtained by quantum chemical computations performed on the molecular model of 1,2,4,5-tetracarboxybenzoic acid dimethyl ester.[31] The latter model mimics the molecular environment of the cross-linking agent PMA after the condensation with the OH groups of cyclodextrins to form the ester bridges of β-CDPMA nanosponges. Recent results[31,33,39] demonstrated that the calculated vibrational profiles of 1,2,4,5-tetracarboxybenzoic acid dimethyl ester well reproduce the experimental Raman and IR spectra of nanosponges in the wavenumber range 1500–1800 cm^{-1} where no interfering vibrational bands[40,41] of cyclodextrins are present. The Raman and IR spectra reported in Fig. 1 were acquired on a sample of β-CDPMA14 nanosponge in the dry state, in order to recognize and assign the vibrational modes of the polymer matrix in the spectral range of interest and before the hydration of the polymer in water.

Based on the wavenumber and relative intensities of the computed peaks, the experimental broad band found at about 1718 cm^{-1} in the Raman spectrum is associated with the stretching vibration modes of the carbonyl groups of the PMA residues and it is generally indicated as ν(C═O). The same vibrational mode appears more intense in the IR spectrum of nanosponges and is centred at about 1720 cm^{-1}. As widely discussed in previous studies,[30,31,33,39,44] this asymmetric band in both Raman and IR spectra can be decomposed into two different components, $\nu(C{=}O)_{ester}$ and $\nu(C{=}O)_{carbox}$, assigned

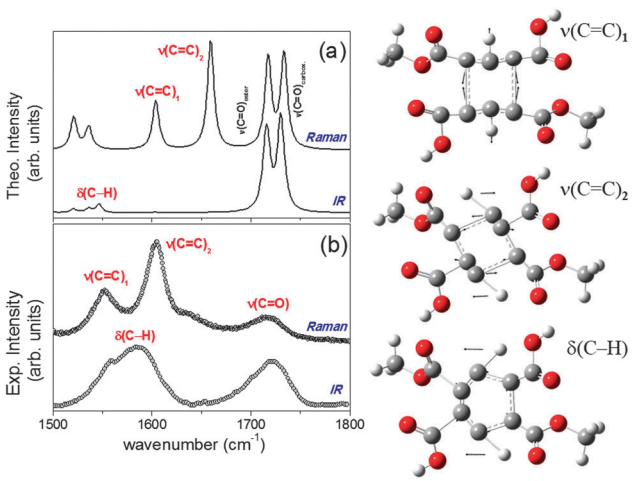

Fig. 1 Theoretical (a) and experimental (b) Raman and IR profiles of the β-CDPMA14 nanosponge in the dry state and in the spectral range 1500–1800 cm^{-1}. Right panel: a schematic picture of the vibrational modes obtained for simulated bridging molecule, namely $\nu(C{=}C)_1$, $\nu(C{=}C)_2$, and δ(C–H).

to the stretching vibrations of the C═O belonging to the ester groups and to the carboxylic groups of PMA, respectively.

The experimental Raman spectrum of the nanosponge polymer shown in Fig. 1 shows the presence of two other intense signals at about 1553 and 1604 cm^{-1}, corresponding to the vibrations labelled as $\nu(C{=}C)_1$ and $\nu(C{=}C)_2$. These modes mainly involve the stretching motions of the C═C bonds of the aromatic ring of PMA, as deduced by the vibrational analysis of the eigenvectors associated with these vibrational energies.[31] However, the displacement of the atoms of PMA, due to the effect of vibrations $\nu(C{=}C)_1$ and $\nu(C{=}C)_2$, is rather different, as clearly evidenced by the picture reported in the right panel of Fig. 1. The vibrational peak found at 1553 cm^{-1} in the experimental Raman spectra ($\nu(C{=}C)_1$) can be essentially described as a ring breathing mode, while the vibration at 1604 cm^{-1} ($\nu(C{=}C)_2$) involves the stretching of the aromatic ring of PMA together with the bending of the C–H groups. These differences are consistent with the theoretical values of the depolarization ratio obtained for the C═C vibrational modes, *i.e.* 0.19 and 0.73 for $\nu(C{=}C)_1$ and $\nu(C{=}C)_2$, respectively, and with the experimental observation that the peak at 1604 cm^{-1} is much less polarized with respect to the band at 1553 cm^{-1}.

It is noteworthy that both modes $\nu(C{=}C)_1$ and $\nu(C{=}C)_2$ exhibit a relatively high Raman activity but they are practically IR-inactive, as deduced by the comparison with the theoretical vibrational spectra shown in Fig. 1(a). Conversely, the IR profile in Fig. 1 exhibits a very intense broad band centred at about 1585 cm^{-1}, labelled as δ(C–H) and assigned to the pure bending modes of the C–H groups of the aromatic ring of PMA residues.

As expected, a significant enhancement of the Raman intensity is observed for the peaks corresponding to $\nu(C{=}C)_1$ and $\nu(C{=}C)_2$ in the spectra excited by using UV radiation (Fig. 1(b)) with respect to the visible light.[31,44] This is due to the resonance occurring at UV wavelengths with the aromatic π–π^* transitions of the ring of PMA residue in nanosponges. These conditions, together with the significant reduction of the interfering fluorescence background achieved by exciting Raman spectra under UV radiation, allow us to detect also slight modifications occurring in the wavenumber position, intensity and the spectral shape of the Raman vibrations associated with the hydrophobic aromatic moiety of the polymer. Moreover, by exploiting a proper line shape analysis of these specific Raman modes it is possible to retrieve additional dynamic information[37,42,43] besides those obtained by a more classic approach, such as the analysis of the shift of the center of mass of the peaks.[31,39,44]

In Fig. 2 we report some representative isotropic Raman profiles obtained for the samples of the β-CDPMA14 hydrogel at different hydration levels *h* and in the spectral range 1400–1800 cm^{-1}. In this specific wavenumber region, the contribution associated with the HOH bending mode of water at about 1640 cm^{-1} exhibits a negligible intensity with respect to the signals associated with the vibration modes of the CDNS polymer. Conversely, the same HOH bending mode of water appears particularly intense in the IR spectra compared to the Raman profile, even at low hydration levels.[39,44]

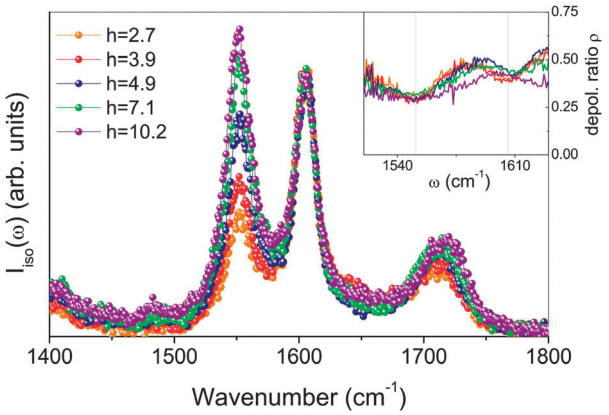

Fig. 2 Isotropic Raman profiles of the β-CDPMA14 hydrogel at different hydration levels *h* in the spectral range 1400–1800 cm^{-1}. Inset: depolarization ratio ρ reported in the restricted spectral range 1520–1630 cm^{-1}.

This experimental finding suggests to focus on the Raman spectra for examining in detail the behaviour of vibration modes associated with the hydrophilic and hydrophobic groups of the water-swollen polymer. At the same time, important information on the state and dynamics of engaged water molecules in the hydrogel matrix can be obtained through the analysis of IR spectra in the same wavenumber window, as discussed in the following.

The experimental profiles of Fig. 2 point out that the increase in the hydration level *h* in the CDNS hydrogel is responsible for a considerable enhancement of $\nu(C{=}C)_1$ intensity. At the same time, a slight shift toward higher wavenumbers is observed on the C═O stretching band upon increasing the water content. The profiles in Fig. 2 were arbitrarily normalized to the intensity of the $\nu(C{=}C)_2$ in order to better emphasize the spectral modifications described above. As a matter of fact, the frequency position, relative intensity and the spectral shape of the $\nu(C{=}C)_2$ Raman peak do not seem to be affected by the variation of the water content in the CDNS hydrogel, thus suggesting the use of this mode as a reliable internal standard. It is noteworthy that the depolarization ratios experimentally estimated for $\nu(C{=}C)_1$ and $\nu(C{=}C)_2$ peaks do not change upon increasing hydration level *h* (see the inset of Fig. 2).

The shift toward higher wavenumbers of the ν(C═O) band with increasing *h* can be explained by taking into account that as the water content increases, the molecules of the solvent at the polymer interface tend to saturate their hydration sites and, subsequently, tend to arrange in a more strongly interconnected hydrogen-bond (HB) network. Consequently, the electrostatic environment experienced by the C═O groups causes a shift toward higher wavenumbers of the CO oscillators. This behaviour is fully consistent with previous results obtained by the analysis of Raman and IR spectra of the CDNS hydrogel[25,33–35] in the high-frequency regime 2700–3700 cm^{-1}. In this spectral region, where the characteristic OH stretching band of water appears particularly intense in both Raman and IR spectra of the hydrogel, the increase of the hydration level was found to lead to

an enhancement of the low-frequency contribution of the OH stretching band, suggesting an increase of cooperativity in the HB pattern of water. On the other hand, a significant reduction of the total intensity of the C═O stretching band together with a slight shift to a higher wavenumber of the band position for high values of h was also observed in the IR spectra of the PMA-nanosponge hydrogel.[39,44]

More interestingly, the observed increase in the intensity of $\nu(C{=}C)_1$ gives evidence that the CH groups of the aromatic ring of PMA are also strongly involved in non-conventional HB interactions of the type C–H···O–H with engaged water molecules. The activation of the hydrogen bond donor character of the CH fragment in the cross-links can be justified by the sp^2 hybridization of the carbon atom. Remarkably, the mode $\nu(C{=}C)_1$ was found to be influenced by the hydration level h to a larger extent than vibration $\nu(C{=}C)_2$, thus providing experimental evidence of the directional character of such interaction, as expected from a genuine hydrogen bond. This point has a direct consequence on the Raman spectra. Indeed, the vibrational mode $\nu(C{=}C)_1$ causes a marked polarizability change in the PMA frame, *i.e.* Raman activity. In turn, the polarizability enhancement is directly related to the HB pattern established with the surrounding water molecules.

A more quantitative description of the h-dependence of the Raman modes $\nu(C{=}C)_1$ and $\nu(C{=}O)$ can be achieved by considering the isotropic Raman profiles of the CDNS hydrogel. The analysis was carried out by following the fitting procedure, based on the Kubo–Anderson model, already successfully applied to other water–organic mixtures.[37,42,43]

Fig. 3 displays some representative best-fit curves of the isotropic Raman spectra of the β-CDPMA14 hydrogel at different hydration levels h.

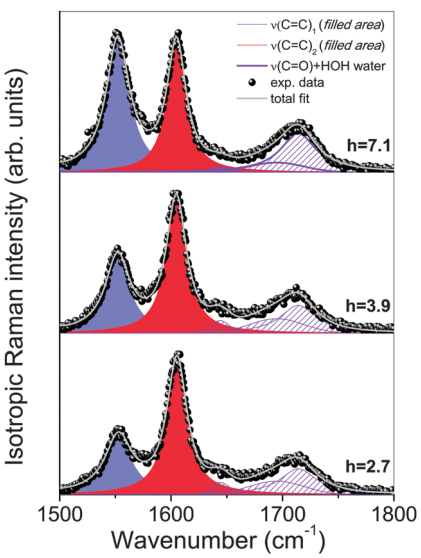

Fig. 3 Some representative results of the fitting procedure of isotropic Raman profiles for the β-CDPMA14 hydrogel at different hydration levels h (black symbols). The total fit curve (grey line) is reported, together with the single components: nanosponge stretching modes $\nu(C{=}C)_1$ (periwinkle filled area) and $\nu(C{=}C)_2$ (red filled area), stretching mode of polymer carbonyl groups and HOH bending mode of water (violet).

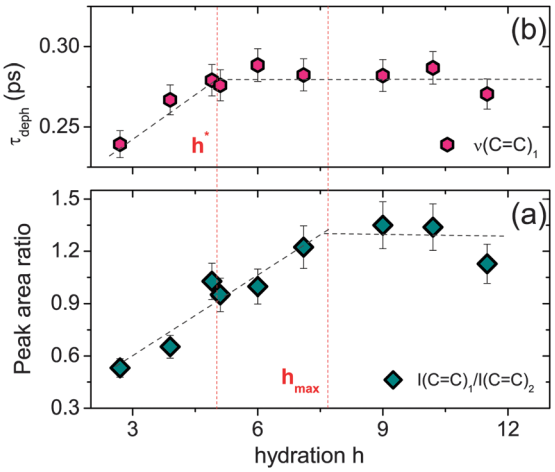

Fig. 4 Hydration-dependence of the $I(C{=}C)_1/I(C{=}C)_2$ area ratio (a) and of the dephasing time τ_{deph} associated with the $\nu(C{=}C)_1$ Raman mode (b) for the β-CDPMA14 hydrogel. Dotted lines are guide to eyes to highlight the h-evolution.

The five KAF functions are used for fitting the data account for the $\nu(C{=}C)_1$ and $\nu(C{=}C)_2$ vibration modes of CDNS, the stretching mode of the carbonyl groups $\nu(C{=}O)_{ester}$ and $\nu(C{=}O)_{carbox}$ and the HOH bending mode of water.

It is noteworthy that in the h-range explored, the peaks corresponding to $\nu(C{=}C)_1$ and $\nu(C{=}C)_2$ are characterized by small values of parameter α, indicating that these modes show a Lorentzian line-shape.

In Fig. 4(a) we report the hydration-dependence of the $I(C{=}C)_1/I(C{=}C)_2$ ratio between the peak areas corresponding to $\nu(C{=}C)_1$ and $\nu(C{=}C)_2$, as obtained by fitting of the β-CDPMA14 hydrogel. A linear increase of this ratio is observed up to about $h_{max} = 8$. Above this value, the intensity of the vibrational peak $\nu(C{=}C)_1$ remains substantially unchanged despite the amount of water increases with respect to the polymer content.

This finding suggests that, at low-hydration levels, the presence of surrounding water molecules strongly perturbs the vibrational dynamics of the CH groups of PMA, as reflected by the experimentally observed changes in the polarizability of the $\nu(C{=}C)_1$ mode. For $h > h_{max} = 8$, the perturbation induced on CH groups of PMA residues by water tends to vanish, probably due to the rearrangement of H_2O molecules in tetrahedral patterns typical of bulk water.

Fig. 4(b) illustrates the h-evolution of the dephasing time τ_{deph} associated with the $\nu(C{=}C)_1$ Raman feature of the β-CDPMA14 hydrogel. This quantity is related to the time during which a molecular vibration loses the initial phase relation of its vibrational amplitude.[37,42,43,45] The vibrational dephasing process is governed by the collisions of the vibration atoms in the medium under the effect of a stochastic perturbation.[45] Therefore, the analysis of the vibrational dephasing processes (*i.e.* estimation of τ_{deph}) can yield new information on the effect of the environmental conditions both on the distribution of the instantaneous vibrational frequency and on the prevalent collision phenomena occurring in the system. In the specific case of vibrational modes of molecules immersed

in HB liquids, like for example organic molecules–water mixtures,[37,42,43] the time period after which the phase memory of the vibrational amplitude of the oscillators is lost due to the effect of the collisions in the liquid. Therefore, in liquid systems the inverse of τ_{deph} represents a reasonable estimation of the collision rate of the solvent molecules on the vibrating chemical groups.[45]

The data in Fig. 4(b) clearly give evidence of the existence of a characteristic point h^* beyond which τ_{deph} stops increasing and becomes approximately hydration-independent. This value can be estimated at about $h^* = 5$. Surprisingly, h^* corresponds to the so-called cross-over hydration level h_{cross} estimated for the β-CDPMA14 hydrogel.[34] Parameter h_{cross} identifies a significant change in the connectivity patterns of the HB of the water molecules engaged in the CDNS hydrogel. Indeed, from the inspection of the OH stretching band in Raman[34] and IR[25,35] spectra of the CDNS hydrogel, it was found that an increase of the hydration leads to an increase of the population of water molecules arranged in tetrahedral HB networks (*i.e.* bulk-like contribution) and, correspondingly, a decrease of the population of water molecules involved in the HB network with connectivity less than four. For $h > h_{cross}$ the population of bulk-like water molecules is favoured with respect to non-bulk-like arrangements.[25,34,35] Recent studies showed that the value of h_{cross} strongly depends on the type of CDNS and it matches in all cases with the value of hydration above which the system evolves from a rigid gel state to a fluid suspension.[25,34,35] The trend of τ_{deph} shown in Fig. 4(b) can be interpreted taking into account the observed change in the viscosity of the β-CDPMA14 hydrogel as a function of hydration.[34] For $h < h^*$ the dephasing time associated with $\nu(C{=}C)_1$ tends to increase consistently with the increasing fluidity exhibited by the hydrogel in this *h*-regime. For $h \geq h^* = h_{cross}$ we observe the complete transition of CDNS from a gel phase to a liquid suspension and, correspondingly, τ_{deph} becomes hydration-independent. From the other hand, the *h*-evolution of τ_{deph} can give a reasonable estimation of the behaviour of the collision rate of the solvent molecules on the vibrating CH groups of the polymer, which is in turn related to the different connectivity patterns of the HB of the water molecules engaged in the CDNS hydrogel. Indeed, the observed decrease of the collision rate at $h < h^*$ can be associated with the progressive rearrangement of water molecules in more cooperative, bulk-like networks as a consequence of saturation sites of the water confinement of CDNS found for hydration levels higher than h_{cross}.[25,34,35]

Fig. 5(a) shows the *h*-evolution of the ratio between the total estimated area of the C═O stretching mode and the area of the $\nu(C{=}C)_2$ peak for the β-CDPMA14 nanosponge hydrogel. Similarly to the behaviour found for $\nu(C{=}C)_1$, we observe a linear increase of the intensity of $\nu(C{=}O)_{tot}$ as a function of water content up to $h_{max} = 4.7 \approx h_{cross}$. These changes in the polarizability of the $\nu(C{=}O)_{tot}$ mode reflect the perturbation induced by the surrounding water molecules on the C═O moieties, as suggested above in the case of perturbation of the vibrational dynamics of CH groups of PMA. However, for $h > h_{max} = 4.7$, the dynamical perturbation induced on C═O groups by water tends to vanish (*i.e.* the ratio $I(C{=}O)_{tot}/I(C{=}C)_2$ becomes hydration-independent), while the same effect occurs at higher values of hydration (*i.e.* $h > h_{max} = 8$) for the CH groups of PMA (see Fig. 4(a)). This difference in the estimated values of h_{max} suggests a picture where the perturbation induced by engaged water molecules on hydrophobic CH groups of PMA appears to be extended over a larger number of hydration shells with respect to the extension of perturbation around the hydrophilic C═O groups of the polymer. This conclusion is fully consistent with the literature data that establish how the hydrophobic groups in aqueous solution have a long-range hydration shell, extending beyond the first neighbour layer,[46] characterized by a different local structure[47] and by a slower dynamics[46] with respect to bulk water.

The value $h = 4.7 \approx h_{cross}$ corresponds also to the hydration level at which the ratio between the peak areas associated with the stretching modes $\nu(C{=}O)_{ester}$ and $\nu(C{=}C)_{carbox}$ shows a minimum, as shown in Fig. 5(b). This occurrence reflects the changes in the polarizability (*i.e.* Raman activity) of the spectral

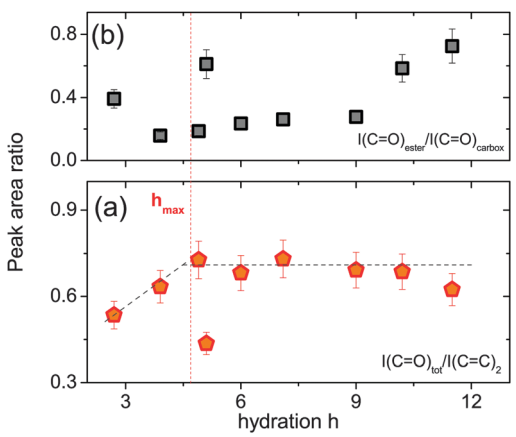

Fig. 5 Hydration-dependence of $I(C{=}O)tot/I(C{=}C)_2$ (a) and of $I(C{=}O)_{ester}/I(C{=}C)_{carbox}$ (b) area ratios. Dotted lines are guide to eyes to highlight the *h*-evolution.

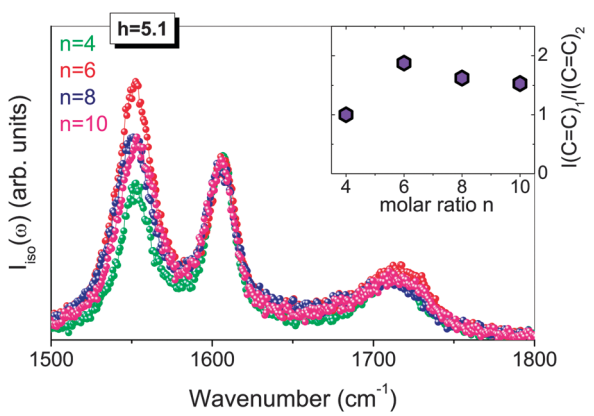

Fig. 6 Isotropic Raman profiles of the β-CDPMA1*n* hydrogel (*n* = 4, 6, 8 and 10) at the same hydration level *h* = 5 in the spectral range 1500–1800 cm^{-1}. Inset: *n*-dependence of the $I(C{=}C)_1/I(C{=}C)_2$ area ratio.

components of the C═O stretching band of nanosponges. It can be explained by considering the different HB acceptor capabilities of the carboxylic groups with respect to the ester groups.[39]

In Fig. 6, the isotropic Raman profiles of different types of β-CDPMA1*n* hydrogels (with n = 4, 6, 8 and 10) are compared at the same hydration level h = 5. As widely discussed in previous studies,[29–33] the molar ratio n strongly affects the degree of reticulation of the CDNS polymer during its synthesis and modulates the elastic properties of the resulting material over the mesoscopic and macroscopic length scale. In particular, it has been found that n = 6 is a critical value where we observe the result of an ideal balance between activated carboxylic groups and free hydroxyl functions onto the cyclodextrin units, leading to the highest interconnectivity between CD cavitands[29–33] in the nanosponge network.

The spectra in Fig. 6 point out a significant difference in the intensity of the $\nu(C{=}C)_1$ mode for different PMA-nanosponges. The inset of Fig. 6 shows the $I(C{=}C)_1/I(C{=}C)_2$ area ratio as a function of n, with the maximum in correspondence of n = 6. This finding suggests that the perturbation introduced by the engaged water molecules in the gel phase on the vibrational motion of hydrophobic CH groups of CDNS is strongly dependent on the cross-linking degree of the polymer, in turn related to parameter n.

In particular, we observe that a more densely cross-linked polymer network undergoes more extended perturbation due to the collision of engaged water molecules with the vibrating aromatic rings of CDNS. On the other side, all our previous investigations give strong indications that the nanosponge polymers obtained for n = 6 are able to entrap much less water with respect to the polymer synthesized under different conditions (*i.e.* $n > 6$ or $n < 6$).[25,35,39,44] The reduced water holding capacity of β-CDPMA16 can be related to the long-range perturbation effect observed for the hydrophobic CH groups of CDNS on the hydration shells formed by engaged water molecules in the gel phase. A picture can be suggested where the minor absorption capacity of nanosponges is regulated, at the molecular level, by an interplay between higher rigidity and reduced dimensions of the pores of the CDNS network[25] and the strong water repulsion operated by the more hydrophobic groups of these systems at n = 6. In this perspective, the balance between hydrophobic and hydrophilic moieties in the chemical structure of the polymer clearly allows for a modulation of the sorption properties of nanosponges, thus adding further elements of versatility to these systems.

All the information on the dynamics of the polymer matrix extracted by the analysis of Raman spectra of the CNDS hydrogel can be related to the structural and dynamical features of the H_2O molecules confined in the gel phase, as derived by the analysis of IR spectra in the 1500–1800 cm^{-1} wavenumber window.

Fig. 7(a) reports the comparison between the IR spectra acquired on the β-CDPMA16 nanosponge hydrated with H_2O and D_2O at the same hydration level h = 0.4. The combined use of deuterated water and H_2O for the swelling of the polymer

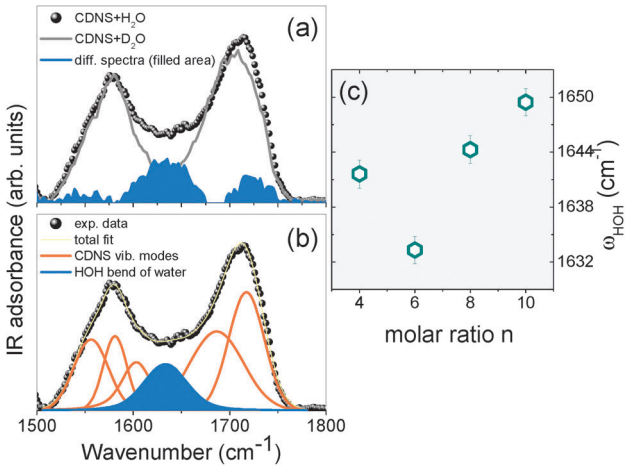

Fig. 7 (a) Infrared spectra obtained for the β-CDPMA16 nanosponge hydrogel (h = 0.4) in H_2O (black symbols) at T = 290 K; the cyan filled line represents the contribution of HOH bending of water, obtained by the subtraction of the signal of the nanosponge hydrogel in D_2O (grey line) (see the text for details). (b) Best-fitting results for the IR spectrum of the β-CDPMA16 nanosponge hydrogel in H_2O; the total fit curve (yellow line) is shown together with the single components: vibration modes of pure CDNS (orange) and HOH bending of water (cyan full line). (c) Estimated position ω_{HOH} of the HOH bending mode of water as a function of molar ratio n at T = 290 K.

allows us to separate, in the IR spectra, the vibration modes assigned to the hydrogel matrix (δ(C–H) and ν(C═O) found at about 1560 and 1714 cm^{-1}, respectively) and the HOH bending mode of engaged H_2O molecules,[48] at about 1640 cm^{-1}. Indeed, it is well known that the DOD bending mode of D_2O is shifted in the vibrational spectra to 1210 cm^{-1}, thus allowing to overcome the severe overlapping between the modes of the polymer and water observed in the 1500–1800 cm^{-1} spectral region.

From the inspection of Fig. 7(a), it is evident that for the experimental profile of the hydrogel prepared with D_2O traces, within the experimental error, the corresponding spectrum in H_2O except for the component of the HOH bending mode, is as expected. This occurrence allows us to isolate the HOH bending mode of confined water by the subtraction of the experimental profile of (CDNS + D_2O) from the corresponding spectrum of (CDNS + H_2O) (Fig. 7(a), filled area). Before the subtraction procedure, the IR spectra in H_2O and D_2O were normalized to the intensity of the band found at about 1030 cm^{-1}, assumed as a reliable internal standard.[30,31,33,39]

The study of the wavenumber position and intensity of the HOH bending mode of water is particularly informative on the state of H_2O molecules confined in the hydrogel matrix. The bending band of water has been suggested to mostly reflect the population of water molecules that do not lie in a symmetric tetrahedral environment, *i.e.* non-bulk-like water molecules.[48]

In order to better quantify the spectral position of the HOH bending mode observed on the raw experimental data, the IR spectra of the H_2O–hydrogel were fitted by using a sum of six Voight functions, as displayed in Fig. 7(b). Five of these functions were used for reproducing the vibrational bands of the

nanosponge matrix[31,33] and one single Voight curve for accounting the presence of the HOH bending mode of water. In order to reduce the number of free parameters during the fitting procedure of the hydrogel spectra, the centre-frequencies of the components associated with the polymer modes were fixed to the values obtained by a preliminary fit of the corresponding D_2O–hydrogel spectra.

Fig. 7(c) shows the *n*-evolution of the wavenumber position ω_{HOH} of the HOH bending mode of water, estimated by the fitting procedure described above, for β-CDPMA1*n* hydrogels.

A clear evolution of wavenumber ω_{HOH} as a function of molar ratio *n* is pointed out in Fig. 7(c), with a minimum value corresponding to $n = 6$. Since a shift toward lower wavenumbers of the HOH bending mode is consistent with a destructuring effect on the HB network of H_2O molecules,[47] the trend of Fig. 7(c) suggests that the hydrogen bond pattern established among the water molecules confined in the pores of the β-CDPMA1*n* hydrogel tends to be maximally disrupted for $n = 6$. This finding is consistent with the more pronounced perturbation of the vibrational dynamics of the hydrophobic groups of CDNS, observed when the polymer network is maximally cross-linked.

Conclusions

The dynamics of the two main components of hydrogel systems, *i.e.* water and polymer matrix, is here explored in the paradigmatic case of water-swollen cross-linked cyclodextrin nanosponges, by the combined use of UV Raman and Infrared experiments. The simultaneous presence, in the structure of CDNS, of hydrophilic and hydrophobic sites mimics the complexity of polysaccharide hydrogels, where the balance between the hydrophilicity/hydrophobicity and the grade of entanglement of the polymer matrix represent the main parameters for tuning the existence of gel- or liquid-like phases.

The modifications of the vibrational dynamics of the CDNS hydrogel was investigated as a function of the hydration level of the polymer in water and of the molecular composition of the matrix, *i.e.* cross-linking density. In this way, the contribution provided by the hydrophobic and hydrophilic groups of water-swollen polymers in the formation of the gel phase was separately accounted and evaluated.

As main results, we found that both hydrophilic C═O groups and hydrophobic CH fragments inserted on the aromatic ring of PMA are sensitive, at the molecular level, to the macroscopic phase changes in the CDNS hydrogel, namely the rigid gel state or liquid suspension. However, the experimental data strongly indicated that the hydrophobic CH groups in contact with surrounding water molecules experience a more pronounced dynamic perturbation with respect to the carbonyl groups due to the collision between the solvent and vibrating atoms of the polymer. This perturbation is consistently reflected by the destructuring effect observed on the hydrogen bond pattern of the water molecules confined in the pores of the nanosponge hydrogel. Additionally, these effects are further amplified by increasing the cross-linking density of the polymer network, as regulated by the molar ratio *n*.

The overall results provided a detailed molecular picture of the swelling phenomena leading to the formation of the gel phase when a chemically cross-linked polymer contacts with water or biological fluids.

Moreover, a general method is proposed here for probing the dynamic behaviour of water and a polymer in complex systems like hydrogels and for describing the connection between the dynamics and structural features of the polymeric backbone. In particular, we demonstrate the great potentiality of UV Raman spectroscopy to retrieve dynamic information, besides their structural counterpart obtained by classical analysis of the basic features of vibrational spectra.

Acknowledgements

We would like to thank Dr Marco Paolantoni for the useful discussions. The authors gratefully acknowledge PRIN 2010–2011 NANOMED prot. 2010 FPTBSH and PRIN 2010–2011 PROxy prot. 2010PFLRJR_005.

Notes and references

1 P. J. Flory, *Principles of polymer chemistry*, Cornell University Press, Ithaca, New York, 1953.
2 N. A. Peppas, Y. Huang, M. Torres-Lugo, J. H. Ward and J. Zhang, *Annu. Rev. Biomed. Eng.*, 2000, **2**, 9.
3 Y. An and J. A. Hubbell, *J. Controlled Release*, 2000, **64**, 205.
4 J. A. Hubbell, *J. Controlled Release*, 1996, **39**, 305.
5 A. C. Jen, M. C. Wake and A. G. Mikos, *Biotechnol. Bioeng.*, 1996, **50**, 357.
6 M. S. Shoichet, *Macromolecules*, 2010, **43**, 581.
7 G. Perale, F. Rossi, M. Santoro, P. Marchetti, A. Mele, F. Castiglione, E. Raffa and M. Masi, *J. Biomed. Nanotechnol.*, 2011, **7**(3), 476.
8 M. Santoro, P. Marchetti, F. Rossi, G. Perale, F. Castiglione, A. Mele and M. Masi, *J. Phys. Chem. B*, 2011, **115**(11), 2503.
9 E. M. Ahmed, F. S. Aggor, M. Awad Ahmed and T. El-Aref Ahmed, *Carbohydr. Polym.*, 2013, **91**, 693.
10 D. A. Rees, *Adv. Carbohydr. Chem. Biochem.*, 1969, **24**, 267.
11 F. A. Aouada, M. R. de Moura, P. R. G. Fernandes, A. F. Rubira and E. C. Muniz, *Eur. Polym. J.*, 2005, **41**, 2134.
12 M. El Fray, A. Pilaszkiewicz, W. Swieszkowski and K. J. Kurzydlowski, *Eur. Polym. J.*, 2007, **43**, 2035.
13 H. S. Mansur, R. L. Orefice and A. A. P. Mansur, *Polymer*, 2004, **45**, 7193.
14 S. Al-Assaf, G. O. Phillips and P. A. Williams, *Food Hydrocolloids*, 2006, **20**, 369.
15 S. Al-Assaf, G. O. Phillips, H. Aoki and Y. Sasaki, *Food Hydrocolloids*, 2007, **21**, 319.
16 F. Cavalieri, E. Chiessi, I. Finelli, F. Natali, G. Paradossi and M. F. Telling, *Macromol. Biosci.*, 2006, **6**, 579.
17 N. Sahiner, M. Singh, D. De Kee, V. T. John and G. L. McPherson, *Polymer*, 2006, **47**, 1124.

18 M. José Moura, M. Margarida Figueiredo and M. Helena Gil, *Biomacromolecules*, 2007, **8**(12), 3823.
19 K. E. Crompton, J. S. Forsythe, M. K. Horne, D. I. Finkelstein and R. B. Knott, *Soft Matter*, 2009, **5**, 4704.
20 F. Hua and M. Qian, *J. Mater. Sci.*, 2001, **36**, 731.
21 F. Trotta, M. Zanetti and R. Cavalli, *Beilstein J. Org. Chem.*, 2012, **8**, 2091.
22 S. V. Chilajwar, P. P. Pednekar, K. R. Jadhav, G. JC Gupta and V. J. Kadam, *Expert Opin. Drug Delivery*, 2014, **11**(1), 111.
23 A. Mele, F. Castiglione, L. Malpezzi, F. Ganazzoli, G. Raffaini, F. Trotta, B. Rossi, A. Fontana and G. Giunchi, *J. Inclusion Phenom. Macrocyclic Chem.*, 2011, **69**, 403.
24 W. Liang, C. Yang, D. Zhou, H. Haneoka, M. Nishijima, G. Fukuhara, T. Mori, F. Castiglione, A. Mele, F. Caldera, F. Trotta and Y. Inoue, *Chem. Commun.*, 2013, **49**, 3510.
25 V. Crupi, D. Majolino, A. Mele, L. Melone, C. Punta, B. Rossi, F. Toraldo, F. Trotta and V. Venuti, *Soft Matter*, 2014, **10**, 2320.
26 L. Seglie, K. Martina, M. Devacchi, C. Roggero, F. Trotta and V. Scariot, *Postharvest Biol. Technol.*, 2011, **59**, 200.
27 D. Li and M. Ma, *Clean Products and Processes*, 2000, **2**, 112.
28 E. Memisoglu-Bilensoy, I. Vural, A. Bochot, J. M. Renoir, D. Duchene and A. A. Hincal, *J. Controlled Release*, 2005, **104**, 489.
29 B. Rossi, S. Caponi, F. Castiglione, S. Corezzi, A. Fontana, M. Giarola, G. Mariotto, A. Mele, C. Petrillo, F. Trotta and G. Viliani, *J. Phys. Chem. B*, 2012, **116**(17), 5323.
30 F. Castiglione, V. Crupi, D. Majolino, A. Mele, B. Rossi, F. Trotta and V. Venuti, *J. Phys. Chem. B*, 2012, **116**(43), 13133.
31 F. Castiglione, V. Crupi, D. Majolino, A. Mele, B. Rossi, F. Trotta and V. Venuti, *J. Phys. Chem. B*, 2012, **116**(27), 7952.
32 V. Crupi, A. Fontana, M. Giarola, S. Longeville, D. Majolino, G. Mariotto, A. Mele, A. Paciaroni, B. Rossi, F. Trotta and V. Venuti, *J. Phys. Chem. B*, 2014, **118**(2), 624.
33 V. Crupi, A. Fontana, M. Giarola, D. Majolino, G. Mariotto, A. Mele, L. Melone, C. Punta, B. Rossi, F. Trotta and V. Venuti, *J. Raman Spectrosc.*, 2013, **44**(10), 1457.
34 V. Crupi, A. Fontana, D. Majolino, A. Mele, L. Melone, C. Punta, B. Rossi, F. Rossi, F. Trotta and V. Venuti, *J. Inclusion Phenom. Macrocyclic Chem.*, 2014, **80**, 69.
35 F. Castiglione, V. Crupi, D. Majolino, A. Mele, L. Melone, W. Panzeri, C. Punta, B. Rossi, F. Trotta and V. Venuti, *J. Inclusion Phenom. Macrocyclic Chem.*, 2014, **80**, 77.
36 F. D'Amico, M. Saito, F. Bencivenga, M. Marsi, A. Gessini, G. Camisasca, E. Principi, R. Cucini, S. DiFonzo and A. Battistoni, *Nucl. Instrum. Methods Phys. Res., Sect. A*, 2013, **703**, 33.
37 F. D'Amico, F. Bencivenga, G. Gessini, E. Principi, R. Cucini and C. Masciovecchio, *J. Phys. Chem. B*, 2012, **116**, 13219.
38 M. J. Frisch, G. W. Trucks, H. B. Schlegel, G. E. Scuseria, M. A. Robb, J. R. Cheeseman, J. A. Montgomery, Jr., T. Vreven, K. N. Kudin, J. C. Burant, J. M. Millam, S. S. Iyengar, J. Tomasi, V. Barone, B. Mennucci, M. Cossi, G. Scalmani, N. Rega, G. A. Petersson, H. Nakatsuji, M. Hada, M. Ehara, K. Toyota, R. Fukuda, J. Hasegawa, M. Ishida, T. Nakajima, Y. Honda, O. Kitao, H. Nakai, M. Klene, X. Li, J. E. Knox, H. P. Hratchian, J. B. Cross, V. Bakken, C. Adamo, J. Jaramillo, R. Gomperts, R. E. Stratmann, O. Yazyev, A. J. Austin, R. Cammi, C. Pomelli, J. W. Ochterski, P. Y. Ayala, K. Morokuma, G. A. Voth, P. Salvador, J. J. Dannenberg, V. G. Zakrzewski, S. Dapprich, A. D. Daniels, M. C. Strain, O. Farkas, D. K. Malick, A. D. Rabuck, K. Raghavachari, J. B. Foresman, J. V. Ortiz, Q. Cui, A. G. Baboul, S. Clifford, J. Cioslowski, B. B. Stefanov, G. Liu, A. Liashenko, P. Piskorz, I. Komaromi, R. L. Martin, D. J. Fox, T. Keith, M. A. Al-Laham, C. Y. Peng, A. Nanayakkara, M. Challacombe, P. M. W. Gill, B. Johnson, W. Chen, M. W. Wong, C. Gonzalez and J. A. Pople, *Gaussian 03, Revision C.02*, Gaussian, Inc., Wallingford CT, 2004.
39 V. Crupi, D. Majolino, A. Mele, B. Rossi, F. Trotta and V. Venuti, *Soft Matter*, 2013, **9**, 6457.
40 V. Crupi, D. Majolino, A. Paciaroni, B. Rossi, R. Stancanelli, V. Venuti and G. Viliani, *J. Raman Spectrosc.*, 2010, **41**(7), 764.
41 V. Crupi, D. Majolino, V. Venuti, G. Guella, I. Mancini, B. Rossi, P. Verrocchio, G. Viliani and R. Stancanelli, *J. Phys. Chem. A*, 2010, **114**(25), 6811.
42 F. D'Amico, F. Bencivenga, A. Gessini and C. Masciovecchio, *J. Phys. Chem. B*, 2010, **114**, 10628.
43 F. D'Amico, F. Bencivenga, G. Camisasca, A. Gessini, E. Principi, R. Cucini and C. Masciovecchio, *J. Chem. Phys.*, 2013, **139**, 01510.
44 F. Castiglione, V. Crupi, D. Majolino, A. Mele, B. Rossi, F. Trotta and V. Venuti, *J. Raman Spectrosc.*, 2013, **44**(10), 1463.
45 W. G. Rothschild, *J. Chem. Phys.*, 1976, **65**, 455.
46 S. Perticaroli, L. Comez, M. Paolantoni, P. Sassi, A. Morresi and D. Fioretto, *J. Am. Chem. Soc.*, 2011, **133**, 12063.
47 C. Petersen, K. J. Tielrooij and H. J. Bakker, *J. Chem. Phys.*, 2009, **130**, 214511.
48 J. B. Brubach, A. Mermet, A. Filabozzi, A. Gerschel and P. Roy, *J. Chem. Phys.*, 2005, **122**, 184509.